

DESY SR-73/9  
November 1973

Optical Properties of Anthracene Single Crystals in the Excitonic Region  
of the Spectrum between 4 and 10.5 eV.

by

E. E. Koch and A. Otto  
*Sektion Physik der Universität München*

DESY-Bibliothek

4. JAN. 1974

To be sure that your preprints are promptly included in the  
HIGH ENERGY PHYSICS INDEX,  
send them to the following address ( if possible by air mail ) :

DESY  
Bibliothek  
2 Hamburg 52  
Notkestieg 1  
Germany

OPTICAL PROPERTIES OF ANTHRACENE SINGLE CRYSTALS IN THE EXCITONIC REGION  
OF THE SPECTRUM BETWEEN 4 and 10.5 eV<sup>+</sup>

by

E. E. Koch and A. Otto  
Sektion Physik der Universität München

Abstract

The optical constants in the photon energy range between 4 and 10.5 eV for  $E \parallel b$  on (001) and  $E \parallel L$  and  $E \perp L$  on the (010)-plane are discussed. In particular the influence of macroscopic fields on the optical properties of anisotropic crystals is considered. For  $E \parallel a$  on the (001)-plane reflection spectra have been measured at various angles of incidence. These data and results obtained recently by Hymowitz and Clark for several artificially prepared crystal faces are discussed on the basis of the frequency dependend dielectric functions. New information on the directional dispersion of exciton bands is thus obtained.

---

<sup>+</sup>Work supported by Deutsches Elektronen-Synchrotron DESY and Deutsche Forschungsgemeinschaft DFG.

## I. Introduction

For the experimental and theoretical study of the electronic properties of molecular crystals, which constitute a large group of insulators and semiconductors, anthracene is regarded as a basic example. Among the possible techniques for investigating the electronic properties of such a highly anisotropic crystal optical studies are of fundamental interest, since a large amount of information can be obtained from them. From the knowledge of the optical properties information can be obtained for instance on the properties of excitons, the energy splitting of the exciton bands due to the crystal field i.e. the Davydov-splitting [1,2] and on the influence of macroscopic longitudinal fields [3,4] on these exciton bands.

Whereas detailed spectroscopic work has been done in order to investigate the first singlet exciton at about 3.1 eV [5-10], less information is available for the higher singlet exciton states having excitation energies above 4 eV. This is probably due to the experimental difficulties encountered in this spectral range. Only within the last several years have optical experiments on anthracene single crystals been carried out in the UV and VUV in order to measure the Davydov splitting near the center of the Brillouin zone ( $\underline{k} \approx 0$ ). In particular, interest was focused on the intense exciton band which originates from the strong  ${}^1B_{2u} \leftarrow {}^1A_{1g}$  electronic  $\pi - \pi^*$  transition of the free anthracene molecule, the excitation energy of which is 5.24 eV (e.g. [11,12]) and whose transition dipole moment is parallel to the long molecular axis. Because the absorption in this spectral range is so strong [13], this  ${}^1B_{2u}$ -exciton has to be investigated by reflection spectroscopy [14,15,16]. It shows a metal like reflection up to 75% for photon energies between 4 and 6 eV [16].

Theoretical calculations of exciton bands involving dipole lattice sums show a singular part at  $\underline{k} = 0$ , which is due to the macroscopic part of the exciton field [3,4,17-19]. These fields are longitudinal, i.e., in the direction  $\frac{\underline{k}}{|\underline{k}|}$ . In the past some confusion in the interpretation of the experimental results was caused, because this singularity was not taken into account - as has been recently emphasized by Philpott and Lee [20]. A combined theoretical and experimental effort by Philpott, Clark and Hymowitz, involving the macroscopic excitation fields and reflection spectra from the natural (001) (20 $\bar{1}$ )( $\bar{1}$ 10)

planes and a set of artificially cut planes containing the  $\langle 010 \rangle$  axis (this is the  $\underline{b}$ -axis) of anthracene single crystals has aided considerably in clarifying the situation [17, 21-27].

We reported earlier on near normal incidence  $\underline{E}$ -polarized reflection spectra from the (001)-face with the electric vector parallel to the  $\underline{b}$ -axis  $\langle 010 \rangle$  and from the (010)-face and many directions of the electric vector [16]. The macroscopic exciton fields disappear for these two cases due to the symmetry of the monoclinic crystal [4,16]. The energy splitting of the  ${}^1B_{2u}$ -exciton peaks in the  $\epsilon_2$ -spectra, which were derived from the reflection data via a Kramers-Kronig analysis, was found to be  $E_{\perp b}(010) - E_{\parallel b}(001) = -0.02 \pm 0.03$  eV. Note the convention, that  $\underline{k}$  is normal to the plane, whose Miller indices are given, and that  $\underline{k} \rightarrow 0$ .

Philpott calculated [28], using a model with 5 excitons, higher multipole interaction terms and the rescaled molecular orbit lattice sums of Silbey, Jortner and Rice [29] a Davydov splitting of  $E_{\perp b}(010) - E_{\parallel b}(001) = 0.01$  eV, which is in very good agreement with the experimental value. The corresponding calculations [24] for  $E_{\perp b}(001)$  and  $E_{\parallel b}(001)$ , yield for the  ${}^1B_{2u}$  exciton  $E_{\perp b}(001) = 6.14$  eV,  $E_{\parallel b}(001) = 4.58$  eV and for the pure longitudinal exciton  $E_{\perp b}^{\text{long}} = 6.92$  eV. The experimental values are  $E_{\parallel b}(001) = 4.58 \pm 0.03$  eV [16] and  $E_{\perp b}^{\text{long}}$  between 6.0 and 6.2 eV (See Fig.9 for comparison). The last value is obtained from  $\text{Im } 1/\epsilon$  spectra (Fig.8) or more directly from electron energy loss measurements [30-33].

For the reflection spectra from the (001) face with  $\underline{E}$  parallel to the  $\underline{a}$ -axis, there occurs an intensity mixing of the  ${}^1B_{2u}$  exciton and the second lowest  ${}^1B_{1u}$  exciton. There is as yet no satisfactory theoretical interpretation of the reflection spectrum [17], which displays two peaks near 5.6 eV and 6.08 eV [16]. The calculated energy  $E_{\perp b}(001)$  of the second lowest  ${}^1B_{1u}$  exciton is 5.38 eV [24].

The aim of the present work was first, to extend the analysis of the existing reflectance data [16]; second, to obtain new experimental information which may help in the theoretical interpretation of the near normal incidence spectra from the (001) face and the electric vector parallel to the  $\underline{a}$ -axis  $\langle 100 \rangle$ ; third to compare this spectrum with the experimental information from spectra of the (010) face [16] by use of a macroscopic dielectric theory [4]; and

fourth to compare the spectra recently obtained by Hymowitz and Clark [23] for a number of artificially prepared crystal faces containing the  $\underline{b}$ -axis and  $\underline{E} \perp \underline{b}$  with the data from the (010) plane, again using the same macroscopic theory.

In Section 2 we comment on some theoretical aspects of macroscopic fields in crystal optics. The experimental procedure is briefly described in Section 3. The results (Section 4) together with spectra measured by Hymowitz and Clark from artificially cut crystal faces [23] are discussed in detail in Section 6, where they are compared to data obtained by means of electron energy loss spectroscopy [30-35] and to the calculations (Section 5) based on the theory of crystal optics [4].

## 2. Theoretical Aspects

Crystalline anthracene belongs to the space group  $D_{2h}^5$  [36]. The projections of the two molecules per unit cell onto the (001) and (010) plane are shown in Fig.1, as well as the direction of the molecular axes  $\underline{L}_1, \underline{L}_2$ , which are the long axes within the plane of the molecules,  $\underline{M}_1, \underline{M}_2$ , the short axes within the plane of the molecules and  $\underline{N}_1, \underline{N}_2$ , which are normal to the molecular planes. Axes  $\underline{L}_2, \underline{M}_2$  and  $\underline{N}_2$  are related to the axes  $\underline{L}_1, \underline{M}_1$ , and  $\underline{N}_1$  by reflection at the (010)-plane and translation  $\langle 1/2, 1/2, 0 \rangle$ .

The dielectric tensor  $\underline{\underline{\epsilon}}(\omega)$  is given for the cartesian system  $\underline{a}, \underline{b}, \underline{c}'$ , corresponding to  $x, y, z$  in Fig.7, by

$$\underline{\underline{\epsilon}}(\omega) = \begin{pmatrix} \epsilon_{aa} & 0 & \epsilon_{ac'} \\ 0 & \epsilon_b & 0 \\ \epsilon_{ac'} & 0 & \epsilon_{c'c'} \end{pmatrix}$$

As discussed in detail in the preceeding paper [4] pure transverse excitations of the crystal are possible for normal incidence on the (001)-plane and the electric vector  $\underline{E}$  parallel to the  $\underline{b}$ -axis and for normal incidence on the (010)-plane.

The equivalent argument in the oriented gas model is the following: If one wants the electric vector of the exciting field to lie parallel to the axes

$\underline{L}_1 - \underline{L}_2$ ,  $\underline{M}_1 - \underline{M}_2$  and  $\underline{N}_1 - \underline{N}_2$ , one has to choose normal incidence on (001) and  $\underline{E} \parallel \underline{b}$ . If one wants the electric vector to lie parallel to the directions  $\underline{L} = \underline{L}_1 + \underline{L}_2$ ,  $\underline{M} = \underline{M}_1 + \underline{M}_2$  or  $\underline{N} = \underline{N}_1 + \underline{N}_2$ , one has to choose normal incidence on the (010) plane and the appropriate direction of the electric vector. Note that  $\underline{L}$ ,  $\underline{M}$  and  $\underline{N}$  are in the (010) plane. However, one encounters a difficulty: For instance for  $\underline{E} \parallel \underline{M}$  (or  $\underline{L}$  or  $\underline{N}$  respectively) there is also a component of  $\underline{E}$  in the directions of  $\underline{L}$  and  $\underline{N}$ , so that not only  $\underline{M}$ -polarized molecular transitions  ${}^1A_{1g} \rightarrow {}^1B_{1u}$  contribute to the crystal excitation, but also  $\underline{L}$  ( ${}^1A_{1g} \rightarrow {}^1B_{2u}$ ) and  $\underline{N}$  ( ${}^1A_{1g} \rightarrow {}^1B_{3u}$ ) polarized transitions. It is exactly this effect, which gives rise to axial dispersion of the dielectric tensor axes, as discussed in detail in the following paper [37].

As may be deduced from the equations in the preceding paper [4], one may completely take care of axial dispersion in reflection spectroscopy. For a full evaluation of the dielectric tensor elements  $\epsilon_{ac}$ ,  $\epsilon_{aa}$  and  $\epsilon_{c'c'}$ , an additional polarization analyzer in the reflected beam is needed. However, there are experimental difficulties for such an experiment because of intensity reasons and lack of polarizers of high transmission for this spectral range.

If axial dispersion is small, the tensor may be approximately diagonalized and the simple equations (16) and (22) for the reflectance from the preceding paper [4] may be used, provided the electric vector of the light normally incident upon the (010)-plane is parallel to the direction of the dielectric tensor axes.

For anthracene these directions are given over a wide frequency range by  $\underline{L}$ , the direction of the projection of the vectorial sum of the long molecular axes onto the  $\underline{ac}$ -plane, and the direction perpendicular to  $\underline{L}$  in the  $\underline{ac}$ -plane. This may be seen from Table 1, where results for the direction of the tensor axis  $\underline{L}$ , as measured by different techniques, are compiled.

From electron energy loss experiments [37], there is evidence for axial dispersion only for frequencies above the frequency range which is investigated in this work.

In a good approximation the  $\underline{\epsilon}$ -tensor has then the following form

$$(2) \quad \underline{\epsilon} = \begin{pmatrix} \epsilon_{\perp} & 0 & 0 \\ 0 & \epsilon_b & 0 \\ 0 & 0 & \epsilon_{\parallel} \end{pmatrix}$$

with respect to the cartesian system given by the  $\underline{L}$  and  $\underline{b}$  direction, where  $\epsilon_{\parallel}$  refers to the direction of  $\underline{L}$ . In this way, excitons, originating from  $\underline{M}$ -polarized  $B_{1u}$  molecular transitions are analysed in reflection spectra from the  $\underline{ac}$ -plane with  $\underline{E}$  perpendicular to  $\underline{L}$ , and the derived  $\epsilon$  spectra for  $\underline{E} \perp \underline{L}$  ( $\epsilon_{\perp}$  spectra). In order to have some clue, on how the results would be changed qualitatively when  $\underline{E}$  is parallel to  $\underline{M}$ , reflection spectra for the electric vector of the incident radiation parallel to  $\underline{M}$  were measured also, and formally Kramers Kronig analysed, though this is not strictly in the sense of the approximation, where the dielectric axes are fixed by the long molecular axis.

Spatial dispersion effects, as discussed in the preceding paper [4] should be negligible, since theoretical exciton band calculations [26] show little dispersion with the magnitude of  $\underline{k}$  near the center of the Brillouin zone.

### 3. Experimental Procedure

#### 3.1 General Set Up

The reflection measurements were performed using the 7.5 GeV electron synchrotron DESY as the radiation source [38]. The high degree of polarization of the synchrotron light makes it an excellent source for spectroscopic measurements where polarized light is needed. The experimental set up is shown in Fig.2. The pre-mirror reflects the light emitted by the electrons in the synchrotron orbit to the monochromator. The basic design of the near normal incidence monochromator in a modified Wadsworth mount and the reflectometer have been described in earlier publications [39,40] as has the subsequent improvement of a vertical dispersion plane [41]. The spectral resolution used in these experiments with Al + MgF<sub>2</sub> coated 600 lines/mm grating blazed at 1200 Å was 2.5 Å. The electric field vector  $\underline{E}$  of the synchrotron light lies perpendicular to the dispersion plane of the monochromator i.e. the plane of the drawing. The degree of polarization of the radiation behind the exit slit of the monochromator was estimated to be better than 0.94 over the whole spectral range.

In the reflectometer, sample and detector could be rotated independently. This permitted spectra to be taken at various angles of incidence. Moreover, the sample and the detector could be rotated around the optical axis of the reflectometer, which made possible measurements of both TE-polarized and TH-polarized reflection spectra. Two solar blind photomultipliers were used, one with a

sapphire window and a CsTe photocathode yielding a useful spectral response in the range 4.0 to 8.5 eV, the other with CsTe photocathode and LiF window (4 to 10.5 eV). With the low energy cut off at 4.0 eV the wellknown fluorescence in the range of 2.7 to 3.2 eV [42] and visible stray light is excluded as an error in the reflectivity signal.

### 3.2 Crystals

As sample materials we used ultrapure anthracene (Princeton Organics, prinz quality, 99.999 mol % purity). The new spectra we report here were measured from solution grown crystals with a well developed (001)-plane approximately 10 x 20 mm in size. The b-direction was easily identified by the shape of the crystals and by a polarimetric method. Before the measurements the crystals showed a mirrorlike surface free from any visible imperfections. During the measurements they were kept in the evacuated reflectometer, causing a slow deterioration of the surface due to a slow evaporation of crystalline material. This lead to an exponential decrease of the reflectance with time. However, the relative spectral dependence of the reflectance, remained unchanged. The results discussed below have been corrected for the time dependent decrease of the reflectance. For the spectra measured on the (010)-face see Ref.[16].

### 3.3 Data Handling

The data obtained with an X-Y recorder were electronically digitalized and processed using a data handling and processing system based on a PDP 8/e computer on line linked to a combined IBM-360/65, 360/75 computer system [43]. The Kramers Kronig Analysis was performed using the programm described by Klucker and Nielsen [44] with the same system.

## 4. Experimental Results

### 4.1 Normal Incidence Spectra for $E \parallel b$ and on (001) and $E \parallel L$ , $E \perp L$ and $E \parallel M$ on (010)

Figures 3 and 4 summarize our experimental results for those cases, where no effects due to longitudinal macroscopic fields are present [4,16]. The left parts of the figures show the measured reflectance and the extrapolations used in the subsequent Kramers-Kronig analysis. For details of the spectra and the Kramers-Kronig analysis see Ref. [16]. In the right hand part of Fig.3

and Fig.4 the derived spectra of the real and imaginary part of the dielectric constant  $\epsilon$  are shown. For the case  $\underline{E} \parallel \underline{L}$  we also plotted the derived energy loss function  $|\text{Im } \epsilon^{-1}|$ . Note how the broad and intense reflection band for  $\underline{E} \parallel \underline{L}$  contracts to a rather narrow band in the  $\epsilon_2$ -spectrum. Further we note that within the experimental accuracy the spectra for  $\underline{E} \parallel \underline{M}$  and  $\underline{E} \parallel \underline{L}$  on the (010)-face are practically the same.

In Table 3 are compiled the peak positions of the prominent maxima for the most important polarization directions and also the maxima in the absorption spectrum of the free molecule [12] and anthracene in n-heptane solution [45]. The limits given for the peak positions are partly due to the fact that one deals with rather broad bands. The main error, however, comes from the changes in the Kramers-Kronig results due to the use of the different extrapolations as described in [16].

#### 4.2 Non-normal Incidence Spectra from (001) with $\underline{E} \parallel \underline{a}$

The reflectivities from the  $\underline{ab}$ -plane obtained for various angles of incidence  $\Theta$  for TH-polarized light incident in the  $\underline{ag}$ -plane are shown in Fig.5. In this figure, all spectra are normalized to the same arbitrary reflectance value for the maximum at about 6.2 eV (peak B). The position of the two main bands in these spectra at about 5.6 eV (peak A) and 6.2 eV (peak B) show a pronounced shift of 0.15 and 0.31 eV respectively to higher energies if the angle of incidence  $\Theta$  goes from  $\pm 15^\circ$  to  $\pm 60^\circ$ . For comparison, Table 2 gives in addition the position of these bands for  $\Theta = 7.5^\circ$  and TE-polarized light [16]. Further, a decrease of the reflectance of peak A as compared to the band B with increasing values of  $|\Theta|$  is observed (Fig. 6). Finally, we note a change in the spectral behaviour, e.g. the splitting of the band A for spectra taken at  $\Theta = \pm 30^\circ$  (for  $\Theta = -30^\circ$  it is somewhat less pronounced, but clearly apparent in the original measured curve). All these changes are the same for positive and negative values of the angle  $\Theta$ . The slight differences in peak position and in the ratio of intensities observed, are considered to be insignificant in view of the rather broad bands and the limits of the experimental accuracy.

## 5. Calculations

As has been discussed in the previous paper [4] the knowledge of the dielectric tensor elements for the three main axes is sufficient to calculate reflectance spectra for other crystal faces and for non normal incidence.

Under the assumptions discussed in Section 2 the expression for the reflectance as a function of the angle of incidence  $\theta$  for a monoclinic crystal in terms of  $\epsilon_{||}$  and  $\epsilon_{\perp}$  is

$$(3) \quad R(\theta) = \left| \frac{\cos\theta - (\epsilon_z - \sin^2\theta)^{1/2} (\epsilon_{||} \cdot \epsilon_{\perp})^{-1/2}}{\cos\theta + (\epsilon_z - \sin^2\theta)^{1/2} (\epsilon_{||} \cdot \epsilon_{\perp})^{-1/2}} \right|^2$$

where  $\epsilon_z = \epsilon_{\perp} \sin^2\alpha + \epsilon_{||} \cos^2\alpha$  with  $\alpha = 29.5^\circ$  [4].

This equation allows us to compare the experimental results for non normal incidence (section 4.2) with the outcome of the reflection measurements on the ac-crystal plane (section 4.1). As input data a set of  $\epsilon_{||}$  and  $\epsilon_{\perp}$  values is needed. Such a set of original reflectance data together with the extrapolations and the derived  $\epsilon$ -spectra is shown in Fig. 4.

The comparison of the spectra for E  $\perp$  L and E  $\parallel$  M shows that there is hardly any difference in the spectra. This means that excitons which are M-polarized, according to the oriented gas model, are described fairly well by the spectra with E  $\perp$  L. So it seems justified to use in the following calculations E  $\parallel$  L and E  $\perp$  L-spectra only, in order to apply the tensor model as described in section 2.

With the help of equation (3) it is also possible to compare experimental results recently obtained by Hymowitz and Clark [23] from normal incidence measurements from several artificially prepared crystal planes containing the b-axis (E  $\perp$  b) with the reflection measurements from the ac-face (Fig. 4). In order to do so, one has to use as angle  $\alpha$ , the angle between the L-direction and the normal of the particular crystal surface, keeping  $\theta = 0$  (normal incidence).

## 6. Discussion

### 6.1 Comparison with energy loss experiments

Before we discuss details of the optical experiments in the next section, we compare briefly in Fig. 8 our results for the main dielectric tensor components with those derived from electron energy loss experiments. Electron energy loss experiments on solid anthracene have been reported by Jäger [34], Kunstreich and Otto [30], Bubnow and Frankevich [35], Venghaus [31] and Koch, Kunstreich and Otto [32] and Schott [51]. In Ref. [34,51] the anisotropy has not been investigated. A quantitative analysis of the spectra measured by Bubnow and Frankevich with 115 eV electrons reflected from the ab-face seems very difficult. In the remaining experiments the anisotropy of the energy loss spectra was studied. Because the energy loss spectra are determined by the dielectric tensor (see Ref. [37] and references therein) it should be possible to deduce the same information from energy loss and optical experiments.

A quantitative comparison of our results is only possible with the results obtained by Venghaus [31], because in the other experiments no attempt was made to deduce the dielectric constants from the experimentally determined spectrum. In Fig. 8 we compare  $|\text{Im } \epsilon^{-1}|$  for the three main axes, each determined independently by optical and electron loss experiment. Comparison via the reflectance or via the  $\epsilon$ -spectra is not possible, for all three axes, since no definite value for the dielectric function  $\epsilon$  could be obtained from the energy loss experiment for the case  $\underline{E} \parallel \underline{L}$  ( $\epsilon_{zz}$  in Ref. [31]) in the energy range around 6 eV.

Inspection of Fig. 8 shows a fair qualitative agreement between the results of both types of experiments. It is apparent that, at least in the excitonic range of the spectrum, the optical method gives more detailed and precise information. It should be mentioned, however, that energy loss spectroscopy has the potential to measure spatial dispersion of exciton bands, as  $\underline{k}$  may be varied independently from  $\omega$ .

### 6.2 Discussion of the spectra with $\underline{k} \perp \underline{b}$ and $\underline{E} \parallel \underline{a}$

It was mentioned already in the introduction that there is as yet no satisfactory theoretical interpretation for the normal incidence spectra from the (001)-face with  $\underline{E} \parallel \underline{a}$ . Further experimental data which need explanation result

from our measurements at non-normal incidence (Fig. 5 and 6) corresponding to a change of  $\theta$  in equation (3) and by Hymowitz and Clark [23] in their normal incidence spectra for different crystal faces containing the  $\underline{b}$ -axis with  $\underline{E} \parallel \underline{b}$ , which corresponds to a change of  $\alpha$  in equation (3). In this section we compare the results of these experiments with the calculated reflectance spectra.

The experimentally observed spectrum at near normal incidence on the  $\underline{ab}$ -face with  $\underline{E} \parallel \underline{a}$  is compared to the calculated reflectance in Fig. 9. For the experimental peaks at 6.08 and 5.67 eV and the shoulder near 4.7 eV there is corresponding structure in the theoretical curve. The main discrepancy is in the magnitude of the absolute reflectivity. It reaches a maximum of 0.23, a value quite well established by different measurements [17], whereas our calculation yields 0.32 for the maximum.

In Fig. 10 the comparison between experiment and calculation for angles of incidence  $\theta = 30^\circ$  and  $60^\circ$  is shown. The calculations reproduce the following experimental observations: The general decrease of the reflectivity at higher  $\theta$ , the relative enhancement of the maximum near 6 eV relative to the one near 5.7 eV and the shift of these maxima to higher energies with increasing angle of incidence  $\theta$ .

In Fig. 11 are shown the peak reflectivities versus angle of incidence  $\theta$ . As the calculated data extend to greater values of  $\theta$  than the measured spectra (Fig. 6) they show clearly the reflectivity minimum at the main azimuth corresponding to the Brewster case for absorbing material.

In Fig. 12 the reflectivities calculated with equation (3) for normal incidence ( $\theta = 0$ ) and the appropriate angle  $\alpha$ , the normal of the reflecting surface makes to the  $\underline{L}$ -direction (see inserts) are shown. They are compared with the corresponding reflectivities from artificially prepared crystal faces containing the  $\underline{b}$ -axis as measured by Hymowitz and Clark [23]. The good agreement concerning the shift of the main structure should be noted, especially in view of the fact that there is no fitting anywhere. The main discrepancy is again in the absolute reflectivity for the  $\underline{ab}$ -face and the face where  $\alpha = 0$ .

The differences in figures 9, 10 and 12 between experimentally determined and calculated reflectance spectra should not be considered as important discrepancies, since it would be possible to obtain a better agreement by scaling

down the absolute reflectance values for  $\underline{E} \perp \underline{L}$  on the  $\underline{ac}$ -plane (Fig. 4), which were used as input data for our calculations. This scaling would still be in the range of our experimental uncertainties of the absolute reflectance.

The good agreement concerning the shift of the main structure shows that one may decide by this type of reflectivity calculation which structure in the  $\underline{ab}$ -face spectra ( $\alpha = 30^\circ$ ) is due to the  ${}^1B_{1u}$ -exciton and which one to the  ${}^1B_{2u}$ , shifted by longitudinal fields towards the frequency of the longitudinal exciton. To this end similar reflection spectra with  $\theta = 0^\circ$  were calculated for closer spaced intervals of the angle  $\alpha$  in steps of  $5^\circ$  (Fig. 13). The peak labeled A does not shift much, finally merging into the M-polarized exciton for  $\alpha = 0$ . One may conclude therefore, that this maximum is mainly due to the second  ${}^1B_{1u}$  M-exciton. The peak labeled B finally disappears giving way to the maximum C, the third  ${}^1B_{1u}$  M-exciton.

In Fig. 14 these observations are summarized. This qualitative picture of the directional dispersion of the various exciton reflection bands is based on our experiments and the calculations. For the sake of simplicity a zero damping was assumed. The dark bands indicate the position of the normal incidence reflection bands with  $\underline{E} \perp \underline{b}$  for various directions of the normal  $\underline{n}$  of the reflecting face with respect to the  $\underline{L}$ -axis. The curved edges of the reflectance bands represent the directional dispersion of the excitons for propagation directions parallel to  $\underline{n}$ . For propagation direction perpendicular to the  $\underline{L}$ -axis one has a broad reflection band extending from approximately 4.5 to 6.1 eV. Because of the interaction of the excitons the crossing of the transverse to longitudinal branches is removed (similar cases are well known from polariton dispersion [49]). This results in a splitting of this reflection band going from  $\underline{n} \perp \underline{L}$  to  $\underline{n} \parallel \underline{L}$ . For  $\underline{n} \parallel \underline{L}$  the lower band is the reflection band extending from the transverse to the longitudinal frequency of the second M-polarized exciton whereas the upper band disappears. For the  $\underline{ab}$ -face, which corresponds to  $\alpha = 30^\circ$ , it is fair to say that the lower reflection band, labeled A in Fig. 5 and 13, is caused by the second M-polarized exciton ( $M_{II}$ ) whereas the upper band B gets all its intensity from the first L-polarized transition ( $L_I$ ).

An independent proof for the assignment of the peak A as being due to the M-polarized exciton comes from reflection spectra at near normal incidence for  $\underline{E} \parallel \underline{a}$  and  $\underline{E} \parallel \underline{b}$  at liquid nitrogen temperature [50]. These measurements

reveal the same vibrational structure for both directions of polarization for the reflection maxima near 5.7 eV, indicating that they both have the same molecular origin.

## 7. Conclusion

The type of analysis which we have presented for the optical spectra of the anthracene single crystal is quite generally applicable to anisotropic molecular crystals. It may thus yield a fairly detailed understanding of the optical properties of a large group of organic solid state systems in their excitonic range of the spectrum.

## Acknowledgement

We wish to thank U. Nielsen and H.W. Wolff for their help in the computational part of the work. Frau Michel-Beyerle kindly provided us with single crystals. We are indebted to L.B. Clark and M.R. Philpott for generously making available to us their results of experiments and calculations prior to publication. Stimulating discussions with them as well as with K.L. Kliewer and S. Kunstreich are gratefully acknowledged.

Table 1

Direction of the main axis of the dielectric tensor as determined by different experimental methods. The angle  $\gamma$  is taken between +a and the main axis L.

angle $\gamma$	m e t h o d	Reference
$120^\circ$	Oriented gas model	Kitaigorodski [36]
$117^\circ$	Optical absorption in the visible ( $h\omega = 2.27$ eV)	Winchell [46]
$119^\circ \pm 3^\circ$	Low frequency capacitive technique	Karl, Rohrbacher and Siebert [47]
$119 \pm 3^\circ$	Electron energy loss	Venghaus [31]
$120 \pm 3^\circ$	UV-reflectance ( $h\omega = 4.90$ eV)	Koch and Otto [16]
$116 \pm 2^\circ$	Low frequency capacitive technique	Munn, Nicholson, Schwob and Williams [48]

Table 2

Position (in eV) of the main reflectance bands as observed for various angles of incidence  $\theta$  and ratio of the reflectance from peak A to peak B.

$\theta$	Peak A	Peak B	R(A)/R(B)
$-60^\circ$	5.75	6.36	60/100
$-45^\circ$	5.60	6.18	70/100
$-30^\circ$	5.56, 5.64	6.11	77/100
$-15^\circ$	5.60	6.05	83/100
$+15^\circ$	5.60	6.05	85/100
$+30^\circ$	5.50, 5.60	6.08	80/100
$+45^\circ$	5.50, 5.62	6.14	72/100
$+60^\circ$	5.75	6.36	52/100
$7.5^\circ$ a)	5.67	6.08	86/100

a) for TE-polarized light, Ref. [16]

Table 3

Position (in eV) of maxima in the absorption spectrum of the free anthracene molecule [11], [12], [32], of anthracene in n-heptane solution [45] and of  $\epsilon_2^-$  and reflection spectra from anthracene single crystals for various directions of polarization (Ref. [16], [17] and this work).

sh : shoulder,  $B_{1u}$  corresponds to short,  $B_{2u}$  to long axis polarized transitions.

Molecule		Single Crystal			
vapour	Solution in n-heptane	$\underline{E} \parallel \underline{b}$ (001)	$\underline{E} \parallel \underline{L}$ (010)	$\underline{E} \perp \underline{L}$ (010)	$\underline{E} \parallel \underline{M}$ (010)
Ref. [11] [12]	Ref. [45]	Ref. [16] [17]			
${}^1B_{1u}$ 3.45±0.1	3.27 ${}^1L_a$	absorption [17] R 3.14 ± 0.03 3.32 3.51	$\epsilon_2$ R - 3.13sh 3.31 3.30 3.52 3.50	$\epsilon_2$ R not measured	$\epsilon_2$ R 3.15±0.03 3.13 3.27 3.29 3.48 3.45
${}^1B_{2u}$ 5.24 5.28 } 0.16 5.40 } 5.56 } 0.16	4.84 ${}^1B_b$	$\epsilon_2$ 4.58±0.03 4.55 4.71 4.70 4.90	4.56±0.03 4.70 4.80 4.95	4.85sh 4.7	4.93±0.03 4.75
${}^1B_{1u}$ ~5.8 5.94	5.62 ${}^1C_b$	5.48±0.05 5.48 ~6.0 5.90sh		5.55±0.05 5.5	5.56±0.05 5.55
${}^1B_{1u}$ ~6.9 ${}^1B_{3u}$ ${}^1B_{1u}$ ~8.1	6.66 ${}^1B_a$	6.33±0.1 6.40 7.6±0.1 7.74 9.25 10.4	7.80 ~9.6	6.30±0.1 6.33 7.05±0.1 7.1 7.6±0.1 7.65	6.30±0.1 6.33 ~7.0 7.05s 7.5±0.1 7.63 9.70 10.65

## References

- [1] A.S. Davydov, J. Exptl. Theoret. Phys. (USSR) 18, 210 (1948)
- [2] For a recent discussion see: V.M. Agranovich, in: Optical Properties of solids, F. Abeles (ed.), p. 315, North Holland, Amsterdam (1972)
- [3] M. Born and K. Huang, Dynamical Theory of Crystal lattices, University Press, London (1954)
- [4] E.E. Koch, A. Otto and K.L. Kliewer, Chem. Phys. preceeding paper
- [5] S.V. Marisova, Opt. Spectr. 22, 310 (1967)
- [6] S.A. Rice, G.C. Morris and W.L. Greer, J. Chem. Phys. 52, 4279 (1970)  
G.C. Morris, S.A. Rice and A.E. Martin, J. Chem. Phys. 52, 5149 (1970)
- [7] J. Schroeder and R. Silbey, J. Chem. Phys. 55, 5418 (1971)
- [8] G.C. Morris, S.A. Rice, M.G. Sceats and A.E. Martin, J. Chem. Phys. 55, 5610 (1971)
- [9] G.C. Morris and M.G. Sceats, Chem. Phys. 1, 259 (1973)
- [10] G.C. Morris and H.G. Sceats, Chem. Phys. 1, 376 (1973)
- [11] E.E. Koch and A. Otto, Opt. Commun. 1, 47 (1969)
- [12] E.E. Koch, A. Otto and K. Radler, Chem. Phys. Letters, in press
- [13] L.E. Lyons and G.C. Morris, J. Chem. Soc. (1959) 1551
- [14] W.H. Wright, J. Chem. Phys. 46, 2951 (1967)
- [15] A. Matsui and Y. Ishi, J. Phys. Soc. Jap. 23, 581 (1967)
- [16] E.E. Koch and A. Otto, phys. stat. sol. (b) 51, 69 (1972)
- [17] L.B. Clark and M.R. Philpott, J. Chem. Phys. 53, 3790 (1970)
- [18] D. Fox and S. Yatsiv, Phys. Rev. 108, 938 (1957)

- [19] V.M. Agranovich and V.L. Ginzburg, *Spatial Dispersion in Crystal Optics and the Theory of Excitons*, Interscience Publ., London (1966)
- [20] M.R. Philpott and J.W. Lee, *J. Chem. Phys.* 58, 595 (1973)
- [21] L.B. Clark, *J. Chem. Phys.* 51, 5719 (1969)
- [22] L.B. Clark, *J. Chem. Phys.* 53, 4092 (1970)
- [23] V. Hymowitz and L.B. Clark, private communication
- [24] M.R. Philpott, private communication
- [25] M.R. Philpott, *J. Chem. Phys.* 50, 5117 (1969)
- [26] M.R. Philpott, *J. Chem. Phys.* 54, 111 (1971)
- [27] M.R. Philpott, *J. Chem. Phys.* 58, 588 (1973)
- [28] M.R. Philpott, *Chem. Phys. Letters* 17, 57 (1972)
- [29] R. Silbey, J. Jortner and S.A. Rice, *J. Chem. Phys.* 42, 1515 (1965)
- [30] S. Kunstreich and A. Otto, *Opt. Commun.* 1, 45 (1969)
- [31] H. Venghaus, *Z. Physik* 239, 289 (1970)
- [32] E.E. Koch, S. Kunstreich and A. Otto, *Opt. Commun.* 2, 365 (1971)
- [33] S. Kunstreich, Dissertation, München (1972)
- [34] J. Jäger, *Ann. Phys.* 22, 147 (1969)
- [35] L.Y. Bubnov and E.L. Frankevich, *Fiz. Tv. Tela* 12, 2164 (1970)
- [36] A.J. Kitaigorodski, *Organic Chemical Crystallography*, Consultants Bureau, New York (1961)
- [37] S. Kunstreich and A. Otto, *Chem. Phys.* following paper
- [38] R.P. Godwin, in: *Springer Tracts in Modern Physics*, vol. 51, p. 1, G. Höhler (ed.), Springer Verlag, Berlin (1969)

- [39] M. Skibowski and W. Steinmann, J. Opt. Soc. Am. 57, 112 (1967)
- [40] G. Rosenbaum, B. Feuerbacher, R.P. Godwin and M. Skibowski, J. Appl. Opt. 7, 1917 (1968)
- [41] E.E. Koch and M. Skibowski, Chem. Phys. Letters 9, 429 (1971)
- [42] K.W. Benz, W. Häcker and H.C. Wolf, Z. Naturf. 25a, 657 (1970)
- [43] U. Nielsen, Interner Bericht, DESY F41-73/2 (1973)
- [44] R. Klucker and U. Nielsen, Computer Phys. Commun., in press
- [45] H.B. Klevens and J.R. Platt, J. Chem. Phys. 17, 470 (1949)
- [46] N. Winchell, The Optical properties of organic compounds, 2ed., Acad. Press, New York (1954)
- [47] N. Karl, H. Rohrbacher and D. Siebert, phys. stat. sol. (a) 4, 105 (1971)
- [48] R.W. Munn, J.R. Nicholson, M.P. Schwob and D.F. Williams, J. Chem. Phys. 58, 3828 (1973)
- [49] L. Merten, in: Festkörperprobleme, Advances in Solid State Physics, Vol. 12, p. 343, O. Madelung (ed.) Vieweg, Braunschweig 1972
- [50] E.E. Koch, A. Otto and V. Saile, preliminary data
- 51 M. Schott, Molec. Cryst. 5, 229 (1969)

## Figure captions

- Fig. 1 Projection of the anthracene unit cell onto the  $\underline{ac}$ - and  $\underline{ab}$ -plane and the projections of the normalized transition moments for long ( $\underline{L}_1, \underline{L}_2$ ) and short ( $\underline{M}_1, \underline{M}_2$ ) axes polarized transitions lying in the molecular plane and for the normal axes ( $\underline{N}_1, \underline{N}_2$ ), together with the projections of the sums and differences of these.
- Fig. 2 Sketch of the experimental set up cut perpendicular to the synchrotron plane.
- Fig. 3 Reflectance spectra of anthracene single crystals for TE-polarized light at near normal incidence ( $7.5^\circ$ ) from the (001)-plane for  $\underline{E} \parallel \underline{b}$  and from the (010)-plane for  $\underline{E} \parallel \underline{L}$  and dielectric functions deduced from them.
- Fig. 4 Reflectance spectra of anthracene single crystals for TE-polarized light at near normal incidence ( $7.5^\circ$ ) from the (010)-plane for  $\underline{E} \parallel \underline{L}$ ,  $\underline{E} \perp \underline{L}$  and  $\underline{E} \parallel \underline{M}$  and dielectric functions deduced from them. For the absolute scale of  $|\text{Im } \epsilon^{-1}|$  see Fig. 8.
- Fig. 5 Reflectance spectra of anthracene single crystals from the (001)-plane for TH-polarized light for various angles of incidence  $\theta$ .
- Fig. 6 Dependence of the  $R_{\text{TH}}$  reflectance for the bands A and B on the angle of incidence  $\theta$ .
- Fig. 7 Conventions of axes and angles used in the calculations. When (001) is the reflecting surface  $\alpha$  equals  $29.5^\circ$ . This case is depicted here. For comparison see figure 1.
- Fig. 8 Comparison of the energy loss function  $|\text{Im } \epsilon^{-1}|$  as obtained from the optical data (solid line) and from energy loss experiments by Venghaus [31] (dashed line).
- Fig. 9 TH-reflectance spectrum of anthracene single crystal at near normal incidence ( $7.5^\circ$ ) from the (001)-plane for  $\underline{E} \parallel \underline{a}$  (solid line) compared to the calculated reflectance using  $\epsilon_{\parallel}$  and  $\epsilon_{\perp}$  as shown in figure 4. Arrows indicate exciton frequencies as obtained by Philpotts calculations [24] (dashed) and by experiment (solid).

- Fig. 10 Comparison between calculated (top) and measured TH-reflectance spectrum (bottom) of anthracene single crystal for angles of incidence  $\theta = 30^\circ$  and  $\theta = 60^\circ$ .
- Fig. 11 Dependence of the TH-reflectance from (001) on the angle of incidence for  $\underline{E} \parallel \underline{a}$  as calculated from (010) reflectance data.
- Fig. 12 Normal incidence reflectance spectra ( $\theta = 0^\circ$ ) of anthracene single crystals for various artificially prepared planes with  $\underline{E} \perp \underline{b}$  according to Hymowitz and Clark [23] (solid line) compared to calculated reflectance using  $\epsilon$ -values derived from (010) reflectance data (broken line). The orientations of the reflecting planes are given as inserts.
- Fig. 13 Reflectance spectra at normal incidence with  $\underline{E} \perp \underline{b}$  on various planes of anthracene single crystals containing the  $\underline{b}$  axis calculated from  $\epsilon_{\parallel}$  and  $\epsilon_{\perp}$ .
- Fig. 14 Qualitative description of the directional dispersion of normal incidence reflectance bands of anthracene for  $\underline{E} \perp \underline{b}$ . Zero damping has been assumed. Transverse (tr) and longitudinal ( $\ell$ ) frequencies of the different L ( $L_I$ ) and M excitons ( $M_{II}$ ,  $M_{III}$ ,  $M_{IV}$ ) are taken from maxima in the experimentally determined  $\text{Im}(\epsilon)$  and  $\text{Im}(\frac{1}{\epsilon})$  spectra.

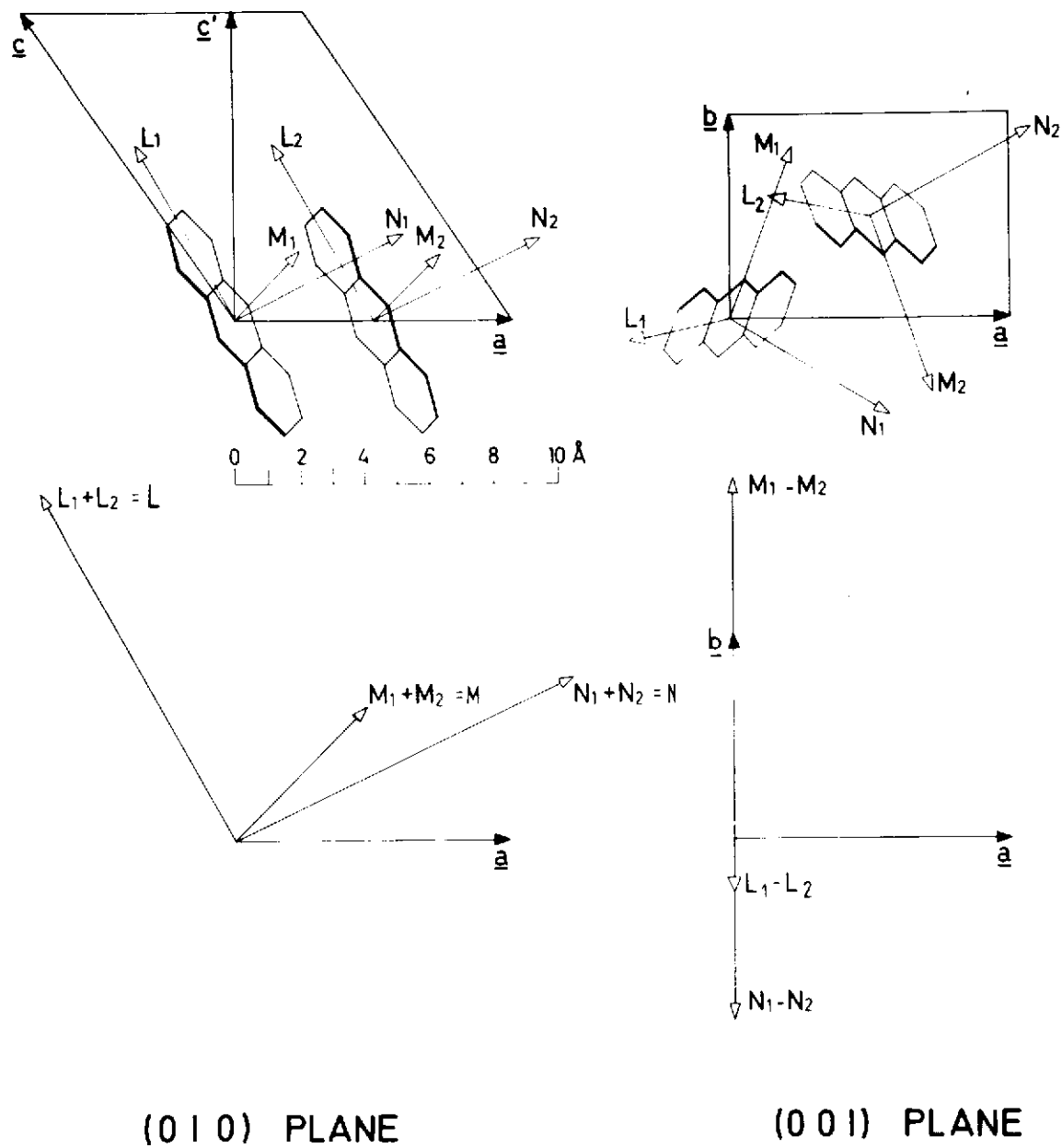


Fig. 1

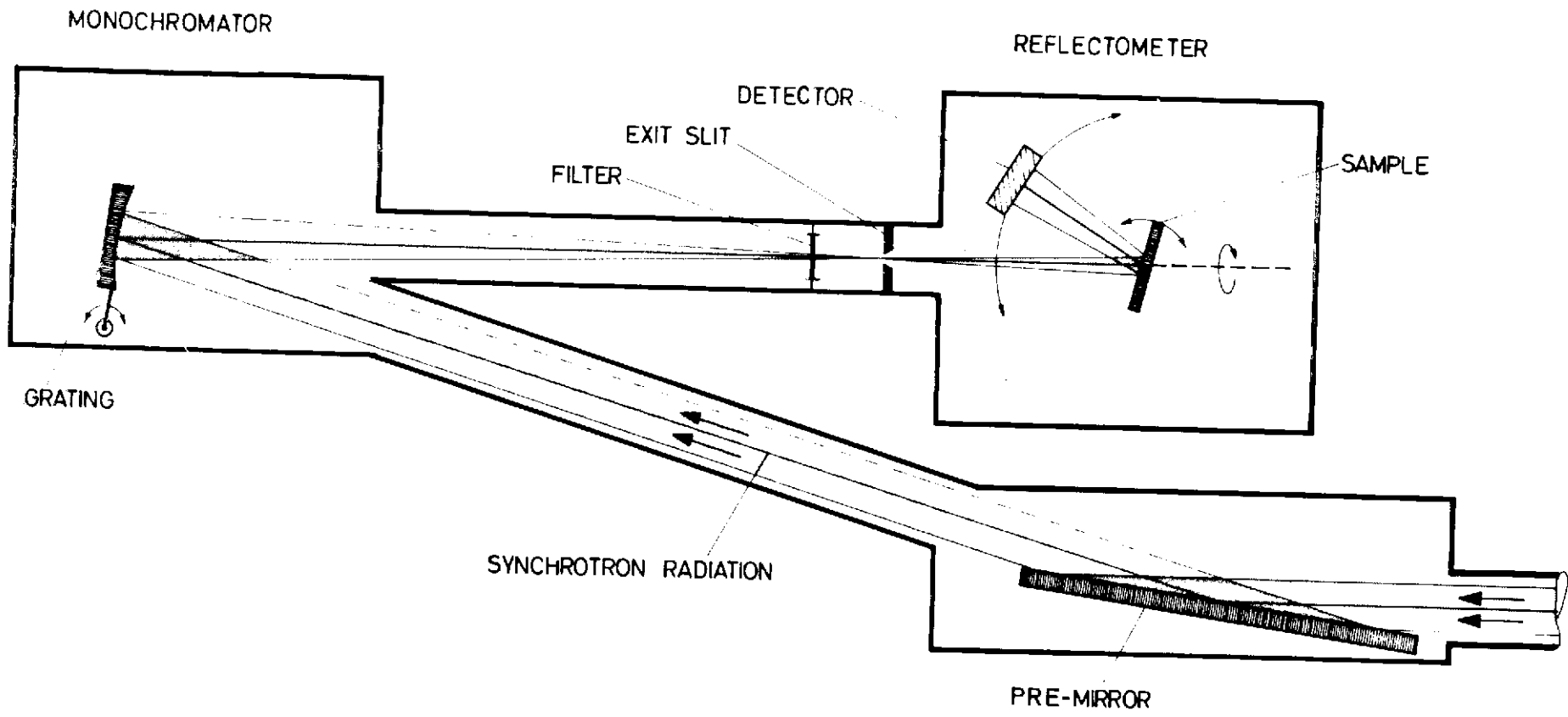


Fig. 2

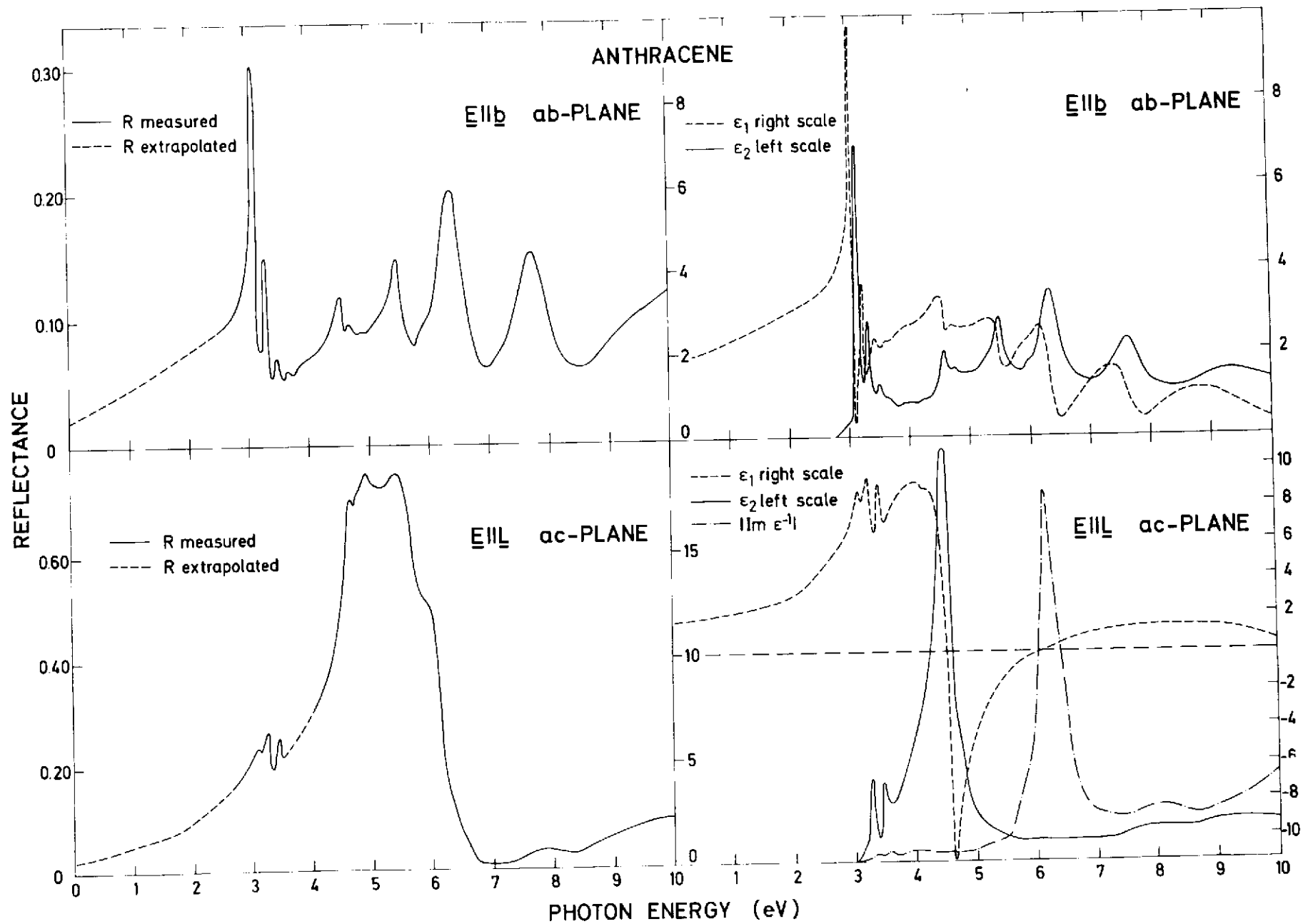


Fig. 3

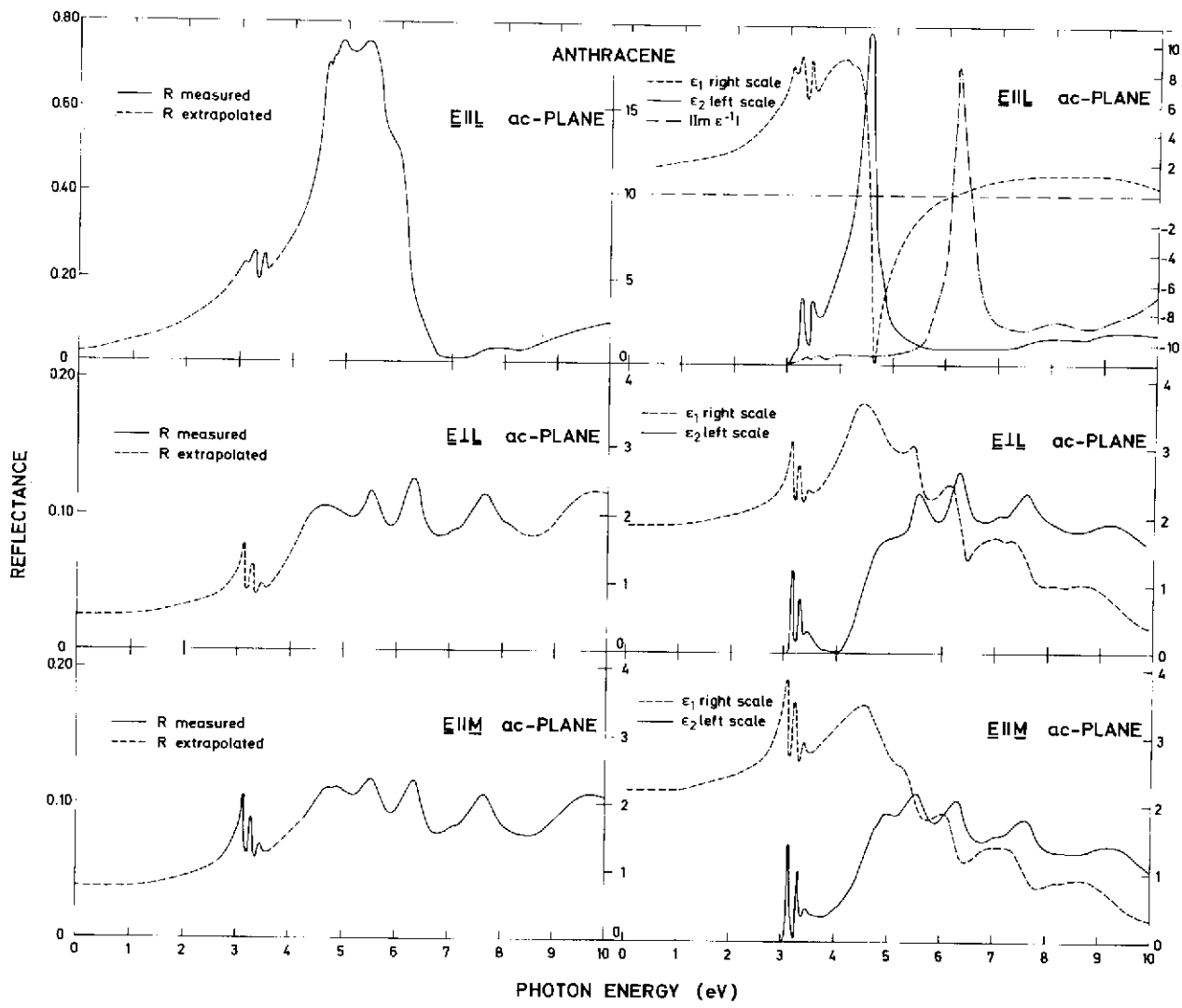


Fig. 4

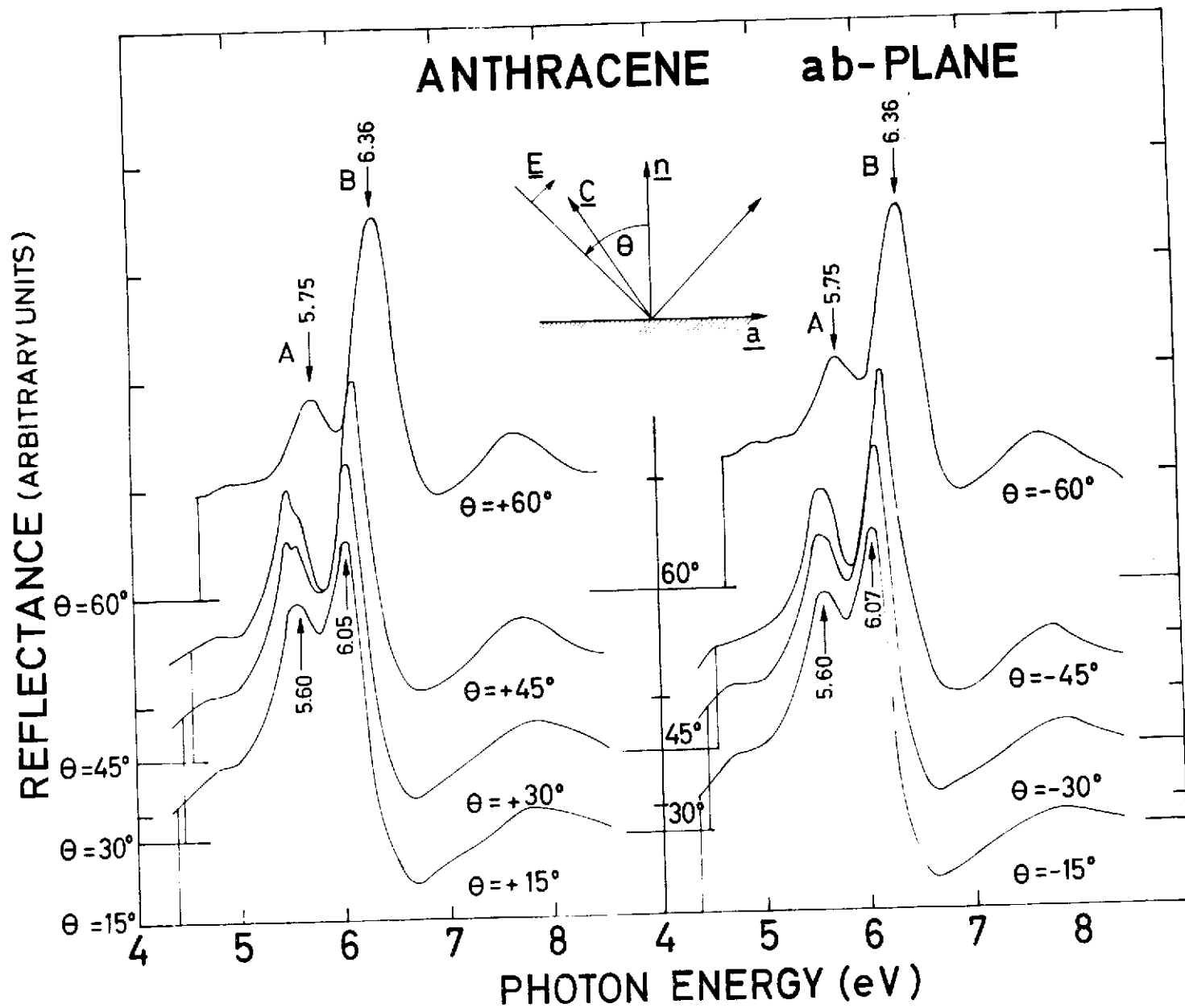


Fig. 5

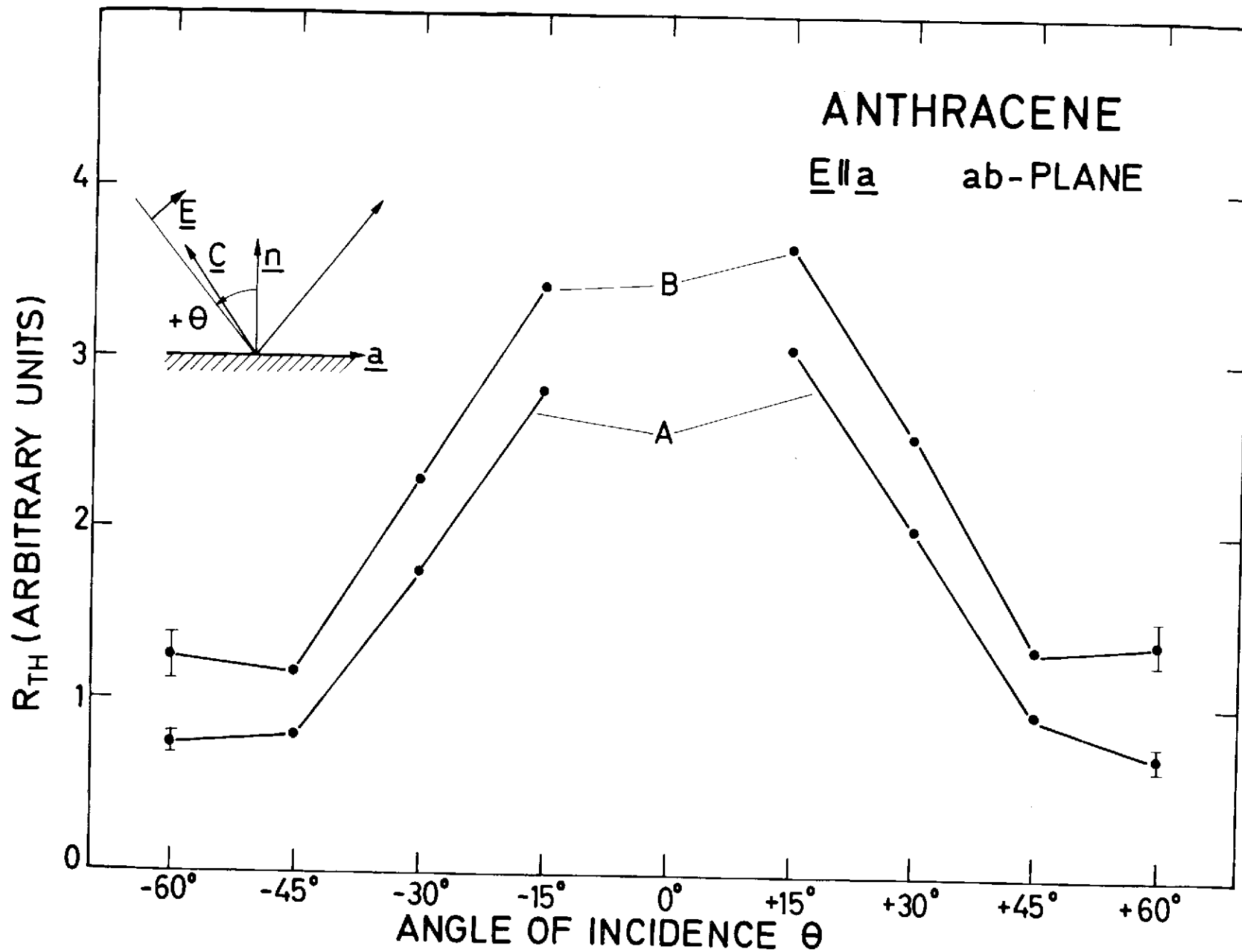


Fig. 6

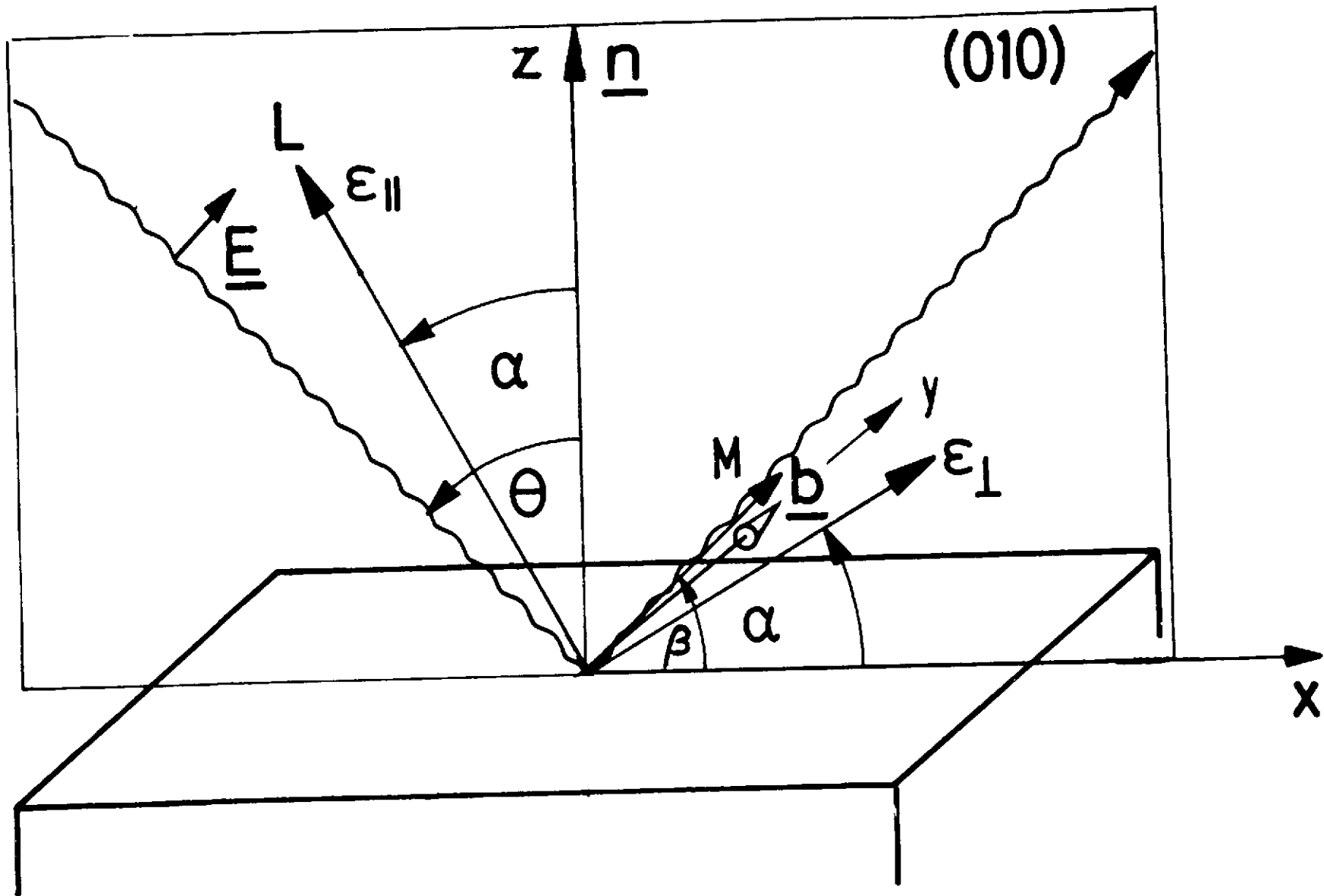


Fig. 7

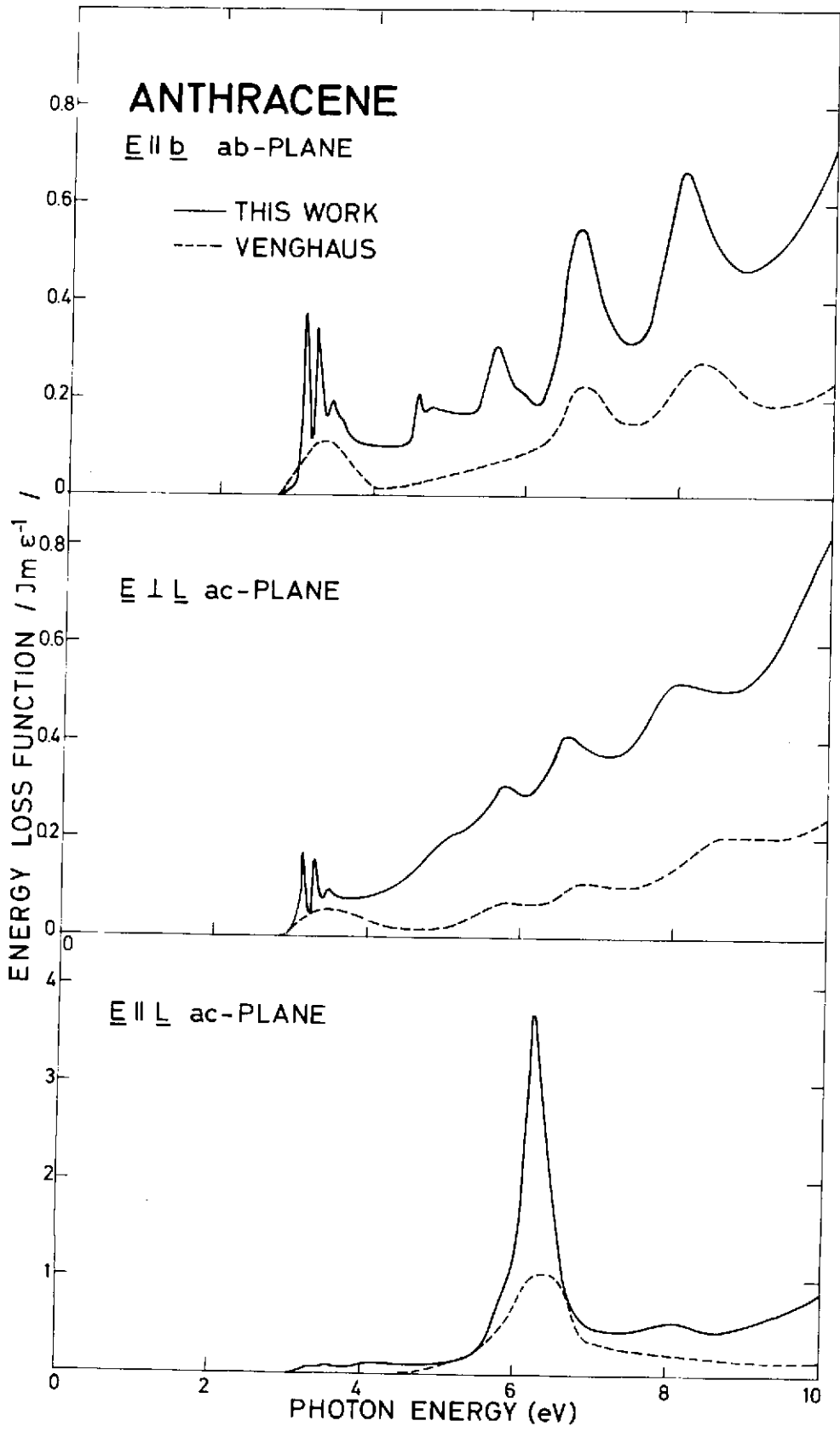


Fig. 8

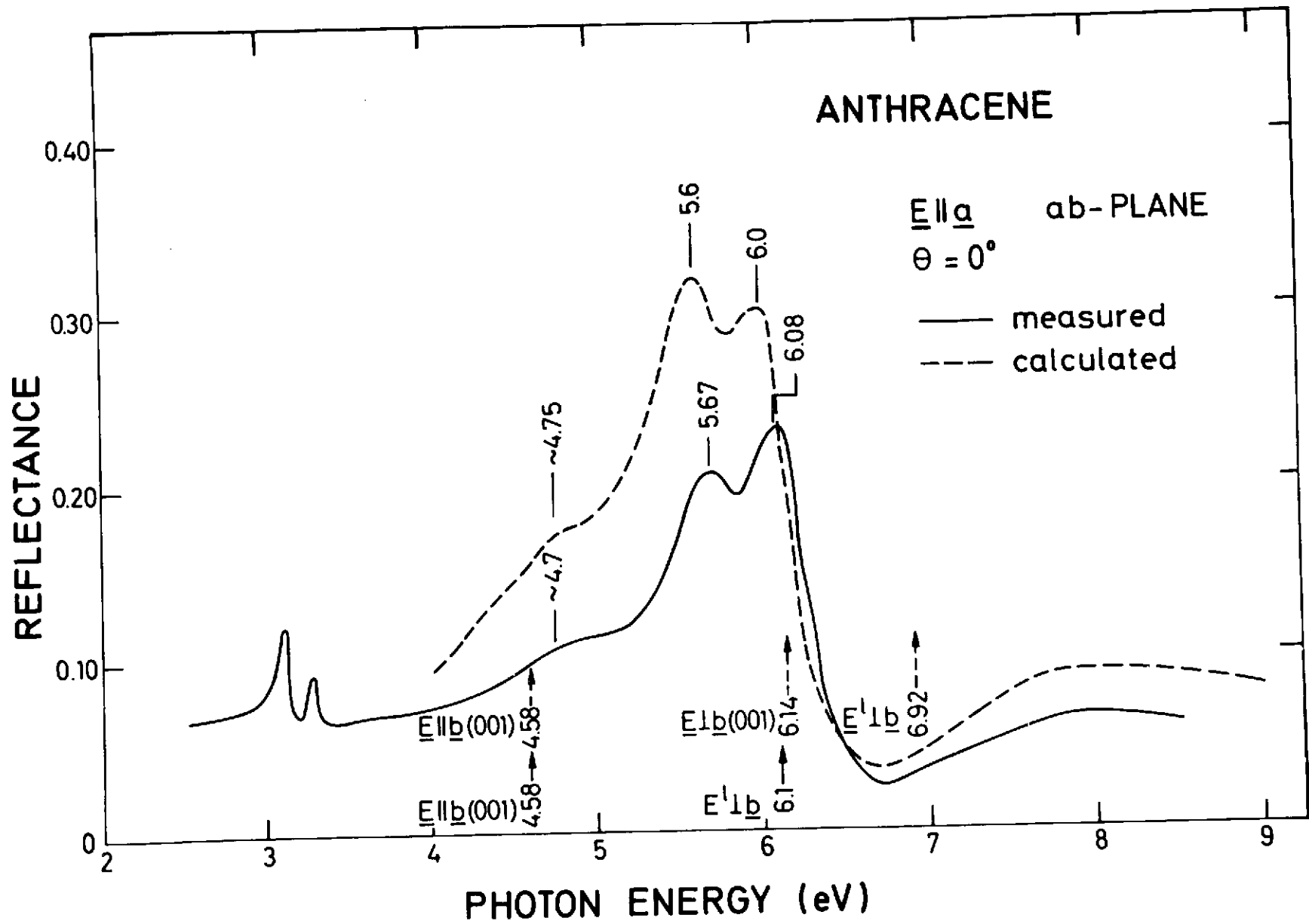


Fig. 9

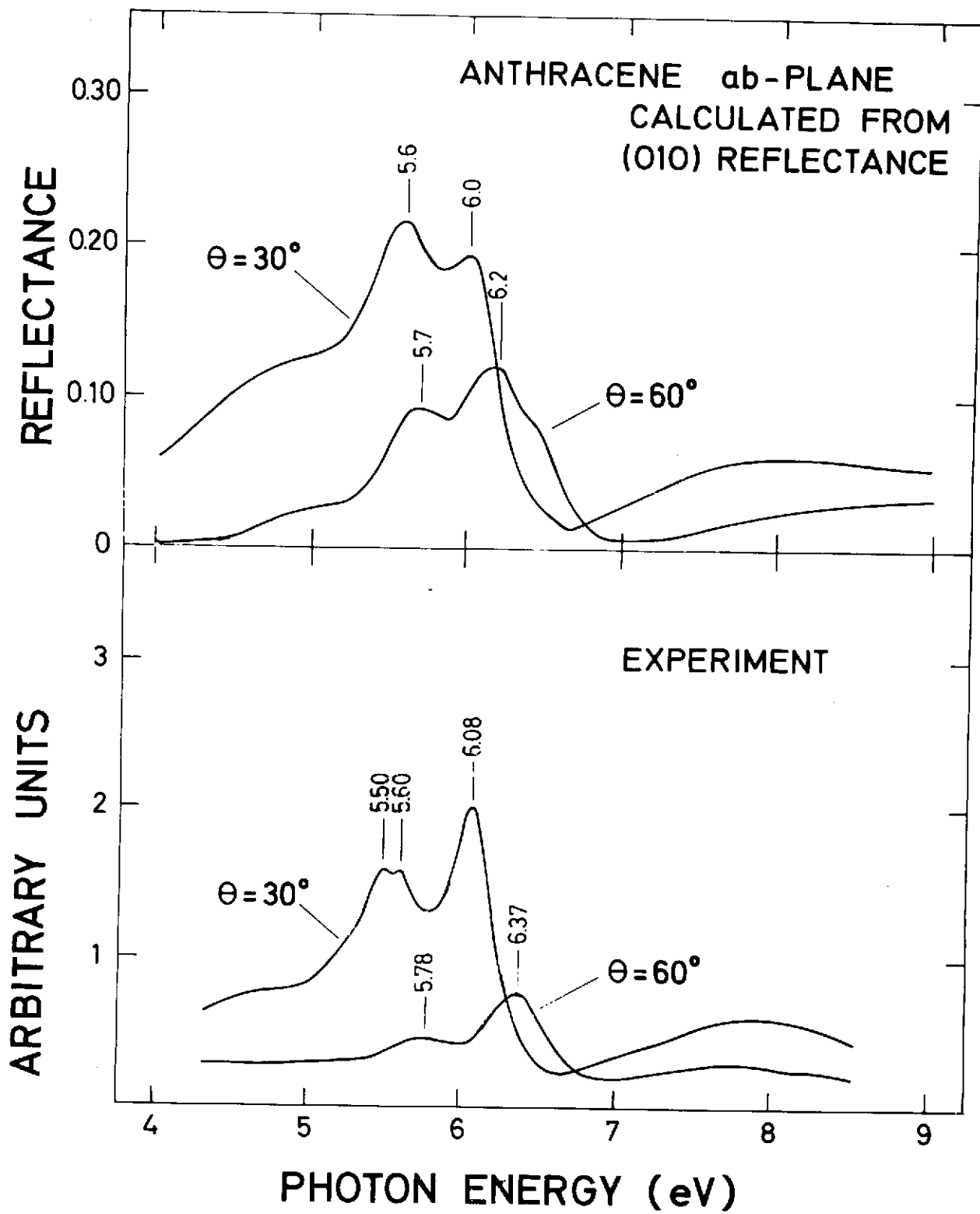


Fig. 10

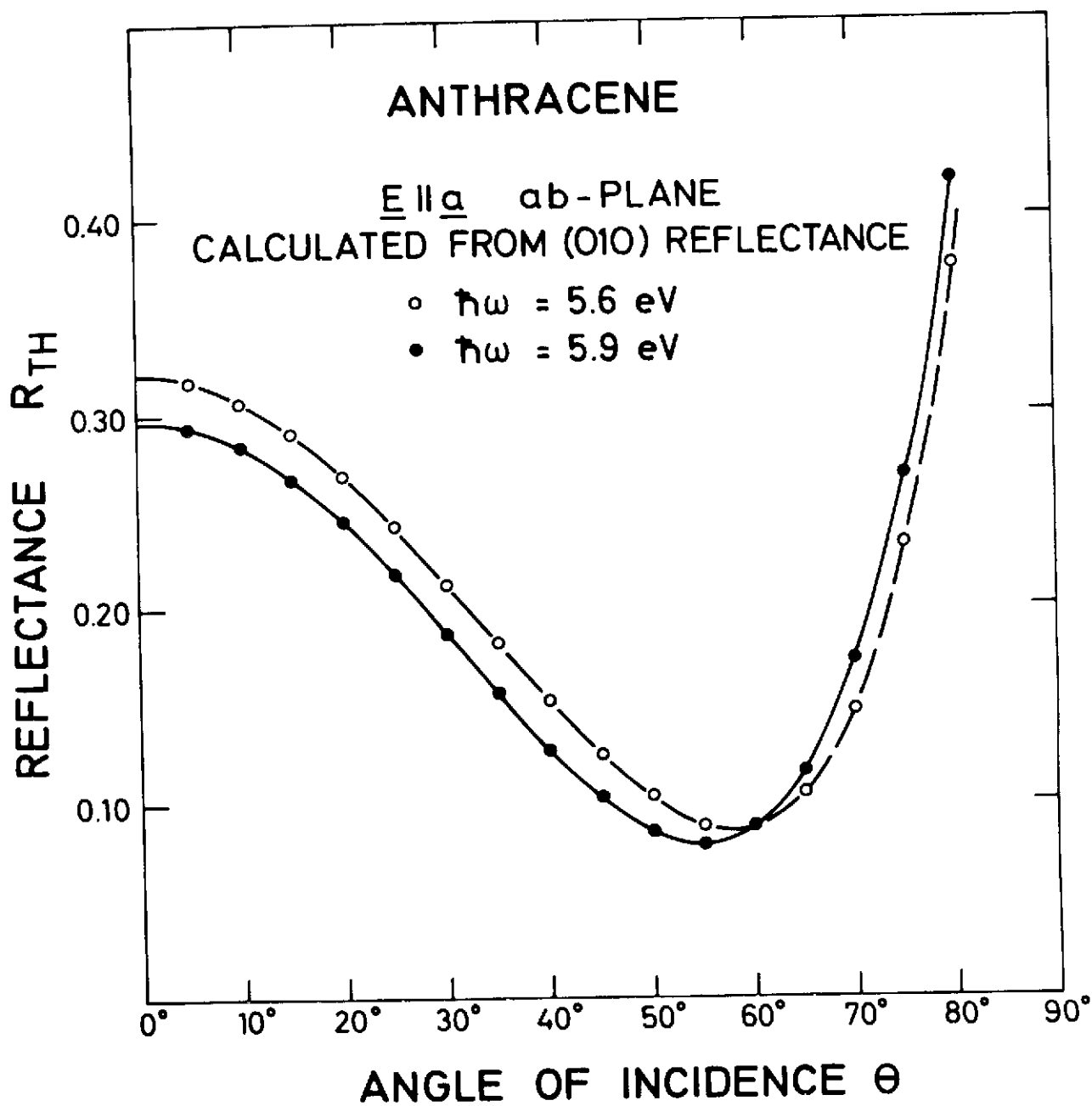


Fig. 11

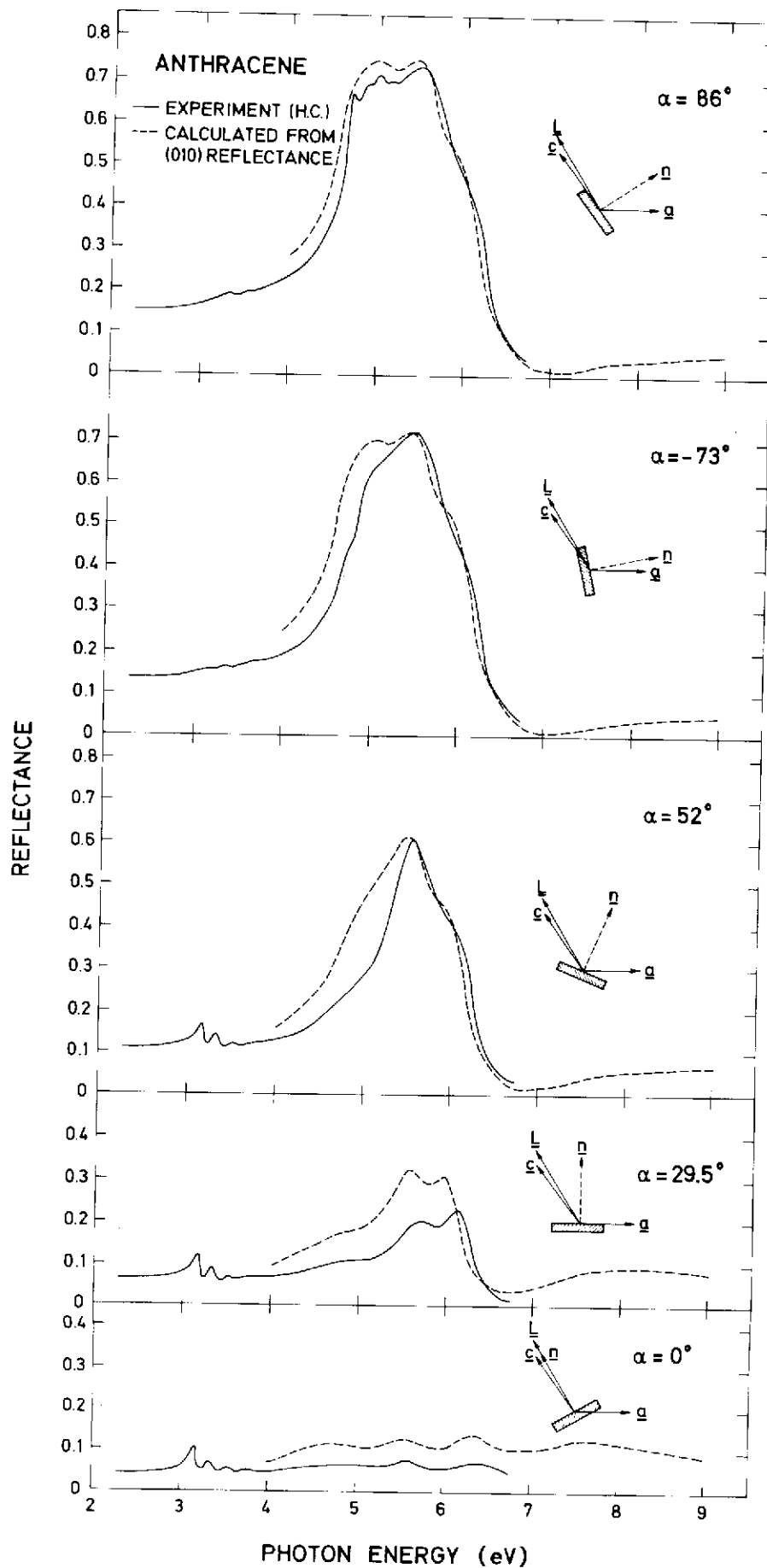


Fig. 12

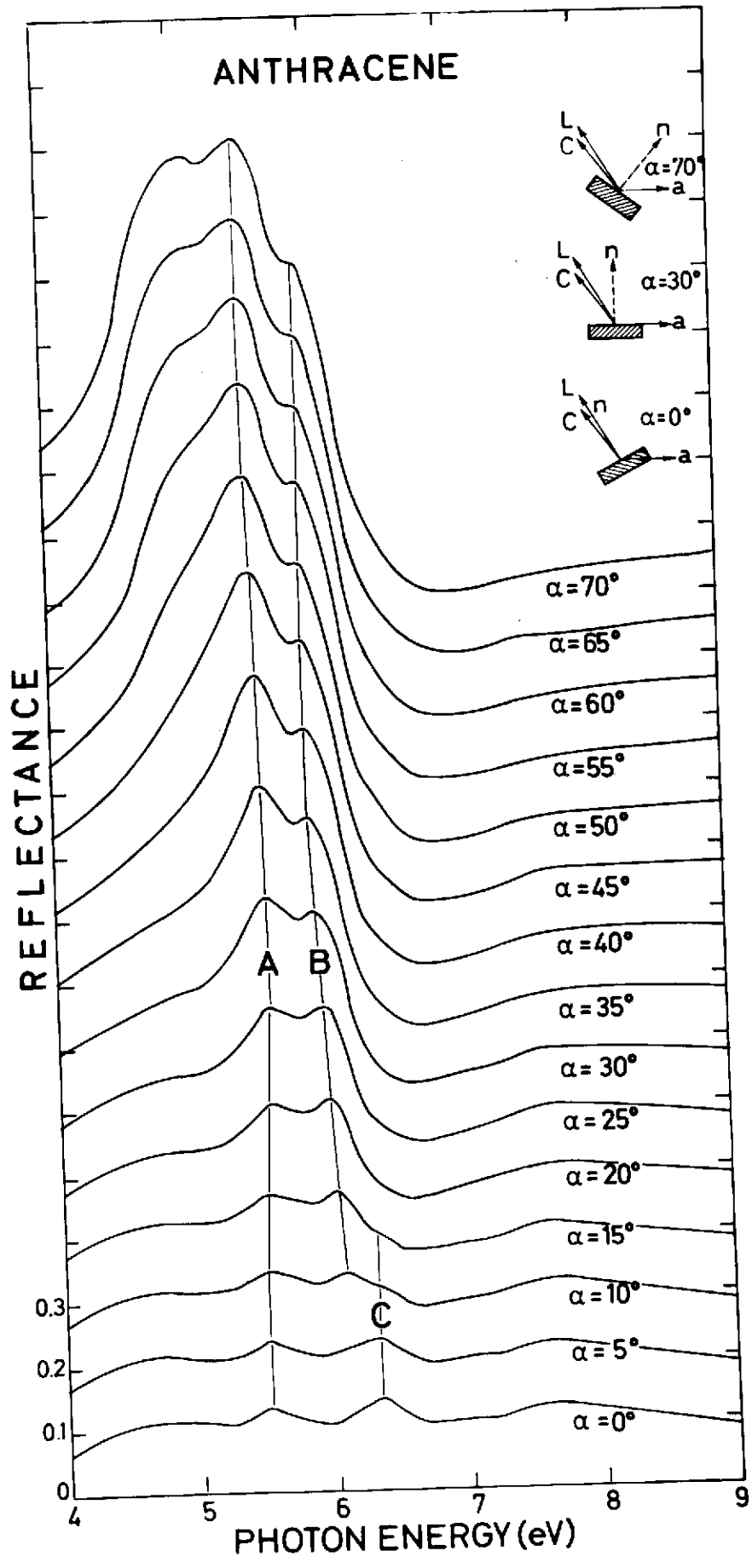


Fig. 13

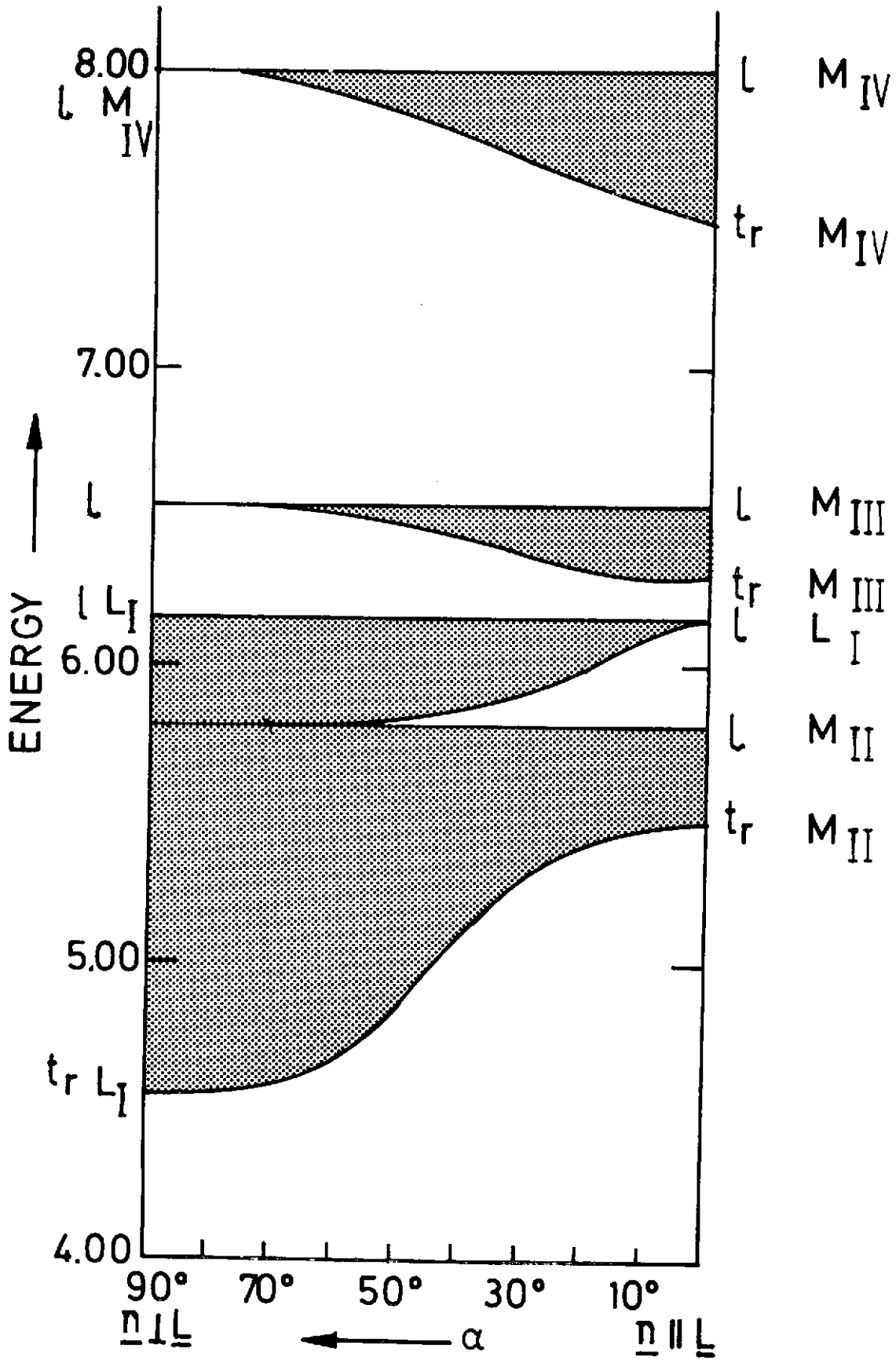


Fig. 14